Chemical Engineering Science 246 (2021) 116984

Contents lists available at ScienceDirect

Chemical Engineering Science

journal homepage: www.elsevier.com/locate/ces

Cu_2O-catalyzed C_2H_2 selective hydrogenation: Use of S for efficiently enhancing C_2H_4 selectivity and reducing the formation of green oil precursor

Li Wang [a,b,1], Bo Zhao [a,b,1], Christopher K. Russell [c,d], Maohong Fan [c,e,f], Baojun Wang [a,b], Lixia Ling [a,b], Riguang Zhang [a,b,*]

[a] State Key Laboratory of Clean and Efficient Coal Utilization, Taiyuan University of Technology, Taiyuan 030024, Shanxi, PR China
[b] Key Laboratory of Coal Science and Technology (Taiyuan University of Technology), Ministry of Education, PR China
[c] College of Engineering and Applied Science, University of Wyoming, Laramie, WY 82071, USA
[d] Davidson School of Chemical Engineering, Purdue University, West Lafayette, IN 47906 USA
[e] School of Civil and Environmental Engineering, Georgia Institute of Technology, Atlanta, GA 30332 USA
[f] School of Energy Resources, University of Wyoming, Laramie, WY 82071, USA

HIGHLIGHTS

- Use of S - a typical catalyst poison enhancing catalytic performance of C_2H_2 selective hydrogenation.
- Sulfur-containing Cu_2O is superior to sulfur-free Cu_2O in C_2H_2 selective hydrogenation.
- Sulfur-containing Cu_2O promotes C_2H_4 formation and inhibits green oil precursor formation.
- S atom modifies Cu_2O surface morphology and tunes the spatial scale of active region for associated reactions.
- S blocks the larger active region required for C_2H_2 polymerization and C_2H_4 hydrogenation.

GRAPHICAL ABSTRACT

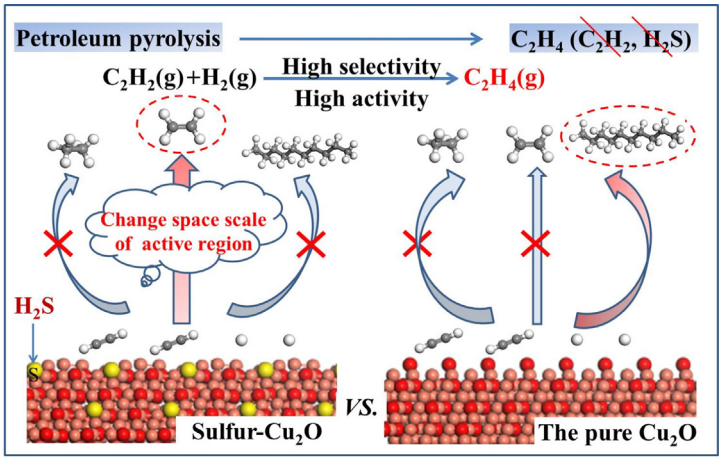

ARTICLE INFO

Article history:
Received 21 November 2020
Received in revised form 14 July 2021
Accepted 27 July 2021
Available online 29 July 2021

Keywords:
Sulfur usage
Cu_2O catalysts
Spatial scale
C_2H_2 selective hydrogenation

ABSTRACT

Development of cost-effective catalysts with high activity and selectivity toward C_2H_2 hydrogenation to gas C_2H_4 is challenging. This research found that the challenge could be overcome using S inherently existing in the raw material for production of C_2H_4 and conventionally considered as a catalyst poison. Specifically, the sulfur-containing Cu_2O catalysts are superior to the sulfur-free Cu_2O catalysts in two dimensions, one is the improvement of C_2H_4 formation activity and selectivity; the other is to reduce green oil precursor formation. The microscopic mechanism of S lies in blocking larger active region required for C_2H_2 polymerization and C_2H_4 hydrogenation to ethane; whereas without affecting smaller active region needed for C_2H_2 hydrogenation to C_2H_4. Namely, the S atom modified Cu_2O surface morphology, change the spatial scale of active region for associated reactions, and control the formation of

* Corresponding author at: State Key Laboratory of Clean and Efficient Coal Utilization, Taiyuan University of Technology, Taiyuan 030024, Shanxi, PR China.
E-mail address: zhangriguang@tyut.edu.cn (R. Zhang).

[1] Represents co-first authors, and contributed equally to this work.

https://doi.org/10.1016/j.ces.2021.116984

Catalytic performance

desired products. Thus, the sulfur-containing Cu_2O catalysts are potentially promising candidates for C_2H_2 hydrogenation to C_2H_4.

1. Introduction

Ethylene (C_2H_4) as a critical polymer building block is dominantly made from the decomposition of higher hydrocarbons. However, during this decomposition process, a small amount of acetylene (C_2H_2) (Beck et al., 2008; True, 2013) and sulfur-containing species (Magyar et al., 2005; Liu et al., 2012; Williams, 2003) are produced. For the former, during C_2H_4 polymerization, C_2H_2 can poison or deactivate the catalysts (Borodziński and Bond, 2006; Borodziński and Bond, 2008). For the later, the high sulfur-containing species (thiophenes and benzothiophenes) are present in the heavier fraction and low sulfur-containing species (H_2S) are present in the light fraction (C_2H_4 feeding stream) (Magyar et al., 2005; Liu et al., 2012). The thiophenes and benzothiophenes can be removed by HDS reaction. However, the elemental sulfur from H_2S dissociation could block surface active sites and poison the metal-based catalysts (Alfonso, 2008; Spencer, 1999; Đnoğlu and Kitchin, 2009). Thus, the coexistence of C_2H_2 and H_2S in C_2H_4 polymerization is not desired.

Nowadays, the selective hydrogenation of C_2H_2 to C_2H_4 is employed for reducing C_2H_2 concentration less than 5 ppm in C_2H_4 feedstock (Zea et al., 2005; Bond, 1962) through simultaneous C_2H_2 removal and C_2H_4 production. The state-of-the-art C_2H_2 hydrogenation catalysts are Pd-based bimetallic catalysts (Borodziński and Bond, 2006; Kim et al., 2011; Khan et al., 2005; Sárkány et al., 2002; Jin et al., 2015). To improve the performance of Pd-based catalyst in C_2H_2 selective hydrogenation, CO was added into feed gas (Borodziński and Bond, 2008; Teschner et al., 2008; Gabasch et al., 2006; García-Mota et al., 2010) to hinder C_2H_4 adsorption and thus increase C_2H_4 selectivity (García-Mota et al., 2010; Nikolaev et al., 2009). Interestingly, pretreating Pd catalysts with sulfur-containing species effectively improve C_2H_4 selectivity, for example, the diphenyl sulphide-modified Pd/TiO_2 catalysts enhances C_2H_4 selectivity without the deactivation (McKenna and Anderson, 2011; McKenna et al., 2011). Pd_4S catalyst showed high C_2H_4 formation activity and selectivity, which were attributed to the unique crystal structure of Pd_4S (McCue et al., 2016; McCue et al., 2017). Pd_4S displayed excellent C_2H_4 selectivity without deactivation or significant carbon deposition (Liu et al., 2018).

The experiment found that PdC_x formation is more of inevitability on Pd catalysts during C_2H_2 semi-hydrogenation (Teschner et al., 2008), moreover, the presence of PdC_x facilitates C_2H_4 desorption to improve C_2H_4 selectivity (Shao et al., 2012; Liu et al., 2020); however, the hydride formation (PdH_x) occurred on Pd catalysts (Sá et al., 2006), which decrease C_2H_4 selectivity in C_2H_2 semi-hydrogenation (Doyle et al., 2004; Khan et al., 2005; Shaikhutdinov et al., 2001). As a result, Cu-based catalysts have attracted increasing attention due to their low cost and high C_2H_4 selectivity (Bridier and Pérez-Ramírez, 2010; Kyriakou et al., 2012; McCue et al., 2014).

Further, a well-known hazard occurs when C_2H_2 contacts with copper or higher copper (I) compounds, because the explosive Cu acetylides would be formed under an alkyne atmosphere. So the application of Cu catalyst in the alkyne process is limited (Garcia and Morse, 2013; Jana et al., 2018). However, the fundamental study of C_2H_2 semi-hydrogenation on the copper (I) compounds in this study is under C_2H_4 atmosphere instead of alkyne atmosphere, which aims to remove the trace C_2H_2 in the C_2H_4 feed, the formation of Cu acetylides might be reduced. Thus, Cu-based catalysts might be applied in the fundamental study of C_2H_2 semi-hydrogenation. On the other hand, the generation of oligomeric species from C_2H_2 polymerization (Wilde et al., 2008), one of the key issues facing for both Pd- and Cu-based catalysts, has not been resolved yet. In particular, compared to Pd catalysts, Cu catalysts are more vulnerable to the threat of oligomeric species since hydrogen dissociation is less facile. As a result, how to reduce the possibility of C_2H_2 polymerization to produce oligomeric species becomes a very key issue on Cu catalysts. These oligomers are the C_{4+} species, and their liquid part is usually called "green oil" (Larsson et al., 1998; Sarkany et al., 1984b,a) that results from the formation of 1,3-butadiene (Asplund, 1996; Larsson et al., 1996, 1998; Yang et al., 2014) and can cause catalyst deactivation, cover the active surface of metal particles, and reduce mass transfer processes such as hydrogen diffusion (Borodzinski and Cybulski, 2000; Teschner et al., 2006).

Cu-based catalysts can contain three valence states of Cu(0), Cu (I) and Cu(II), which have been used for the selective hydrogenation of C_2H_2 (Huisgen, 1963; Lee et al., 2013; McCue et al., 2014; Zhong, 2011), at 423 ~ 523 K, they can present the great selectivity and activity toward C_2H_4 formation (McCue et al., 2014). Under H_2 atmosphere and within 423 ~ 523 K, Cu_2O and Cu are major existing species (Maimaiti et al., 2014; Zhong, 2011). However, Cu_2O(I) catalyst has higher selectivity and activity toward C_2H_4 formation than the single Cu(0) catalyst (Zhang et al., 2017). More importantly, the S species dissociated from a trace amount of sulfur-containing species (H_2S) in C_2H_4 feeding stream can easily be formed over Cu_2O(I) surface during C_2H_2 hydrogenation, for example, our previous DFT studies (Zhang et al., 2012) fully elucidated H_2S adsorption and dissociation on the perfect and oxygen-vacancy $Cu_2O(1\,1\,1)$, H_2S exists in the form of molecular adsorption on the perfect surfaces; H_2S dissociative adsorption occurs on the oxygen-vacancy surface, the produced S atom is preferably adsorbed at the $O_{vacancy}$ site to form sulfurized $Cu_2O(1\,1\,1)$ surface; further, a smaller barrier of molecular adsorption H_2S dissociation into S and H species showed the easy breaking of the H-S bond of H_2S to form S species. The experiment found that H_2S dissociative adsorption on $Cu_2O(1\,1\,1)$ easily occurs (Galtayries and Bonnelle, 1995). The variable-energy photoelectron spectroscopy (Lin et al., 1992) also found that H_2S chemisorbed on $Cu_2O(1\,1\,1)$ could be completely dissociated to produce sulfide, HS and hydroxide. Thus, the S species dissociated from H_2S can easily be formed over Cu_2O surface.

Inspired by the positive effect of S addition to Pd catalysts on C_2H_2 hydrogenation (McKenna and Anderson, 2011; McKenna et al., 2011; McCue et al., 2016; McCue et al., 2017; Liu et al., 2018), this study was desired to investigate the feasibility of Cu_2O(I)-catalyzed C_2H_2 selective hydrogenation using density functional theory (DFT) calculations, which is from the perspective of the effect of S on the catalytic activity and C_2H_4 selectivity as well as reducing the formation possibility of 1,3-butadiene—the precursor of green oil. Four types of $Cu_2O(1\,1\,1)$ surfaces, including the perfect, oxygen-vacancy, the sulfurized and pre-sulfur-adsorbed surfaces, were examined. The results were expected to provide a good clue for designing Cu-based catalysts with higher catalytic performance in C_2H_2 selective hydrogenation.

2. Computational details

2.1. Computational methods

All DFT calculations were performed using Dmol^3 program package in Materials Studio 8.0. The generalized gradient approximation (GGA) with the exchange–correlation functional PBE proposed by Perdew-Burke-Ernzerhof was employed (Delley, 1990; Tian et al., 2007). In the computation, 2.0×10^{-5} Ha, 4.0×10^{-3} Ha•Å^{-1} and 5.0×10^{-3} Å were set for the energy convergence, maximum force and maximum distance, respectively. To expand the valence electron function, the double numerical basis set with a polarization *d*-function (DNP) was selected (Delley, 1990). A $4 \times 4 \times 1$ *k*-point sampling in the surface Brillouin zone was used for $Cu_2O(1\,1\,1)$ and sulfurized $Cu_2O(1\,1\,1)$ surfaces. The orbital cutoff range was set as medium quality, and 0.005 Hartree was set for the smearing value. An effective core potential (ECP) was used for Cu atoms and all-electron basis sets for other atoms.

To obtain accurate activation barriers of elementary reaction involving in the selective hydrogenation of C_2H_2 and the formation of green oil precursor, the transition state (TS) of every elementary reaction was searched using the complete LST/QST method (Govind et al., 2003; Halgren and Lipscomb, 1977). All transition states were confirmed with only one imaginary frequency, and using TS Confirmation to make sure that the transition state was connected with the reactant and product.

Usually, the temperature was set to $\leq$ 400 K for Pd-based catalysts, for example, Yang *et al.* (Yang et al., 2013) theoretically investigated C_2H_2 hydrogenation on several Pd surfaces ((1 1 1), (1 0 0), (2 1 1), and (2 1 1)-defect) at 350 K; Wang *et al.* (Wang and Yang, 2018) examined the effects of lattice strain and subsurface promoters of Pd-based catalysts on C_2H_2 hydrogenation at 350 K; García-Mota *et al.* (García-Mota et al., 2010) experimentally explore the effect of CO on the formation of carbide and hydride phases under the realistic conditions at 348 K; DFT studies by Wang *et al.* (Wang et al., 2021) explore C_2H_2 hydrogenation over the Pd intermetallic compound at 400 K. On the other hand, for Cu-based catalysts, the atomically dispersed Cu supported on a defective nanodiamond-graphene exhibits excellent catalytic performance toward C_2H_2 semi-hydrogenation at 473 K (Huang et al., 2019); the experiment explored the performance of C_2H_2 hydrogenation on Cu-promoted Pd catalysts at 573 K (Kim et al., 2011); Zhang *et al.* (Zhang et al., 2019a,b) explore C_2H_2 hydrogenation on the M@Pd and M@Cu (M = Au, Ag, Cu, and Pd), as well as the promoter Ni, Ag, Au, Pt, Pd and Rh doped Cu-based catalysts at 520 K. Thus, in this study, the temperature 525 K was considered, correspondingly, the entropies of gaseous H_2, C_2H_2, and C_2H_4 species at 525 K are considered.

Further, the hydrogenation and polymerization processes are included in C_2H_2 semi-hydrogenation. The hydrogenation process mainly produces C_2H_4 and C_2H_6, so C_2H_4 selectivity and its formation activity are determined by the hydrogenation process; the polymerization process mainly forms green oil to deactivate the catalyst, thus, the stability of the catalyst is determined by the polymerization process. Further, extensive studies found that the higher H_2/C_2H_2 ratio could reduce the possibility of green oil formation and reduce the possibility of catalyst deactivation in C_2H_2 semi-hydrogenation (Huang et al., 2019; McCue et al., 2014; Wang and Yang, 2018; Yang et al., 2013; Zhang et al., 2019). Thus, in the fundamental study, when exploring the effect of the S on C_2H_4 selectivity and its formation activity, a higher H_2: C_2H_2 ratio (10: 1) was set, the partial pressures of C_2H_2, H_2, and C_2H_4 correspond to 0.01, 0.1, and 0.89 atm, respectively. Moreover, the H_2: C_2H_2 ratio was only considered when calculating the reaction rate using the two-step model method and it did not affect the calculation of the polymerization process in this study. The detailed descriptions about the calculations for Gibbs free energies of gaseous and adsorbed species, the activation free energy and reaction free energy of the involved reaction are presented in the Supplementary Material.

2.2. Calculated models

Previous studies (Islam et al., 2009; Schulz and Cox, 1991) showed that the non-polar stoichiometric O-terminated Cu_2O (1 1 1) surface is the most stable and the dominantly exposed surface under realistic conditions due to the lower surface free energy, which has been widely selected as an ideal model system to investigate the stability, structure and properties of Cu_2O catalysts theoretically (Islam et al., 2009; Sun et al., 2007, 2008) and experimentally (Lin et al., 1992; Önsten et al., 2009; Schulz and Cox, 1991). Thus, the perfect $Cu_2O(1\,1\,1)$ surface named as ***Per-Cu$_2$O(1 1 1)***) was considered and terminated by an outer atomic layer of oxygen anions, with a second atomic layer of Cu^+ cations, and a third atomic layer of oxygen anions. The perfect $Cu_2O(1\,1\,1)$ surface includes four different surface atoms denoted as Cu_{CUS}, Cu_{CSA}, O_{SUF} and O_{SUB} (see Fig. 1a).

On the other hand, metal oxide surfaces under the realistic conditions are not always perfect and usually contain surface vacancies, which can considerably affect the properties of most metal oxides, including surface reactivity (Yin et al., 2007). Zhang *et al.* (Zhang et al., 2010, 2011, 2013, 2017) proved that the oxygen-vacancy $Cu_2O(1\,1\,1)$ exhibits a strong chemical reactivity toward the adsorption and dissociation of H_2S, H_2O, O_2 and H_2. Thus, the oxygen-vacancy $Cu_2O(1\,1\,1)$ surface was selected to investigate the effect of surface oxygen-vacancy on the formation of C_2H_4 and 1,3-butadiene. For the oxygen-vacancy $Cu_2O(1\,1\,1)$ surface or ***O$_V$-Cu$_2$O(1 1 1)***, one oxygen on top atomic layer is removed from the perfect surface as presented in Fig. 1b. The formation energy (E_f) of one surface oxygen vacancy for O_v-$Cu_2O(1\,1\,1)$ is calculated by the equation of $E_f = [E(O_v\text{-}Cu_2O) + 1/2E(O_2)]\text{-}E(Cu_2O)$, in which $E(Cu_2O)$ and $E(O_v\text{-}Cu_2O)$ are the total energies of the clean Cu_2O surface and O_v-$Cu_2O(1\,1\,1)$ surface with one surface oxygen vacancy, respectively; $E(O_2)$ is the energy of a gas phase O_2 molecule. The E_f of O_v-$Cu_2O(1\,1\,1)$ with one surface oxygen vacancy is 2.29 eV, which is close to the values (2.18 and 2.22 eV) obtained by Yu *et al.* (Yu et al., 2015) and Wu *et al.* (Wu et al., 2012). Obviously, the presence of oxygen vacancy gives rise to a threefold site of singly-coordinate Cu^+ cations represented with Cu_2, Cu_3 and Cu_4 atoms.

As presented in Introduction, the dissociated S atoms can adsorb at the oxygen-vacancy sites of $Cu_2O(1\,1\,1)$ surface (Zhang et al., 2012) to form sulfurized $Cu_2O(1\,1\,1)$ surface or ***S$_V$-Cu$_2$O (1 1 1)*** as displayed in Fig. 1c. However, when S atoms adsorbed at the oxygen-vacancy sites, other H_2S species adsorbed at the Cu_{CUS} site can also dissociate, which leads to the adsorption of S atoms at the 3-fold hollow sites composed of one Cu_{CUS} and two Cu_{CSA} atoms and formation of the pre-sulfur-adsorbed $Cu_2O(1\,1\,1)$ surface, as shown in Fig. 1d. This surface is named as ***S$_{ad}$-Cu$_2$O (1 1 1)***.

Therefore, in this study, four types of $Cu_2O(1\,1\,1)$ surfaces, including the perfect, oxygen-vacancy, the sulfurized and pre-sulfur-adsorbed surfaces, have been examined. A $p(2 \times 2)$ supercell slab model with six atomic layers was employed for these surfaces during calculations. The vacuum region separating the slabs in the direction perpendicular to the surface direction was set to 15 Å. In all calculations, the adsorbed species and the top three atomic layers of the substrate were allowed to relax, whereas the bottom three atomic layers of the substrate were frozen in their bulk positions.

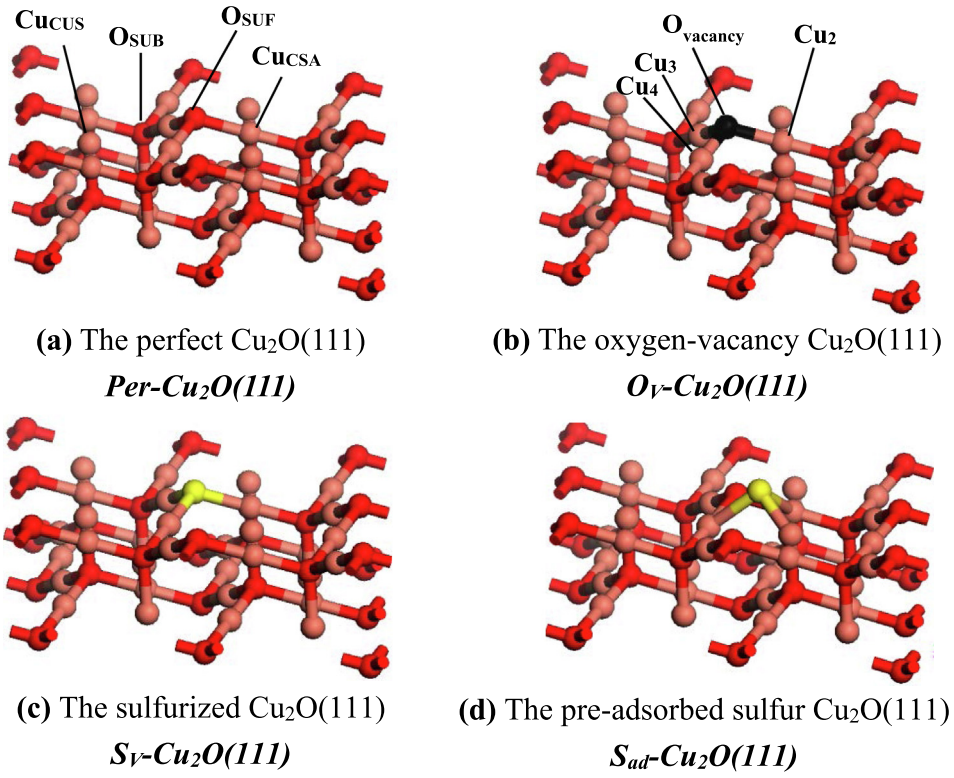

Fig. 1. Surface morphology of (a) the perfect $Cu_2O(1\,1\,1)$, (b) the oxygen-vacancy $Cu_2O(1\,1\,1)$, (c) the sulfurized $Cu_2O(1\,1\,1)$, and (d) the pre-adsorbed sulfur $Cu_2O(1\,1\,1)$, which are named as Per-$Cu_2O(1\,1\,1)$$O_V$-$Cu_2O(1\,1\,1)$$S_V$-$Cu_2O(1\,1\,1)$ and S_{ad}-$Cu_2O(1\,1\,1)$ surfaces, respectively. The red, yellow and orange balls denote O, S and Cu atoms, respectively. (For interpretation of the references to colour in this figure legend, the reader is referred to the web version of this article.)

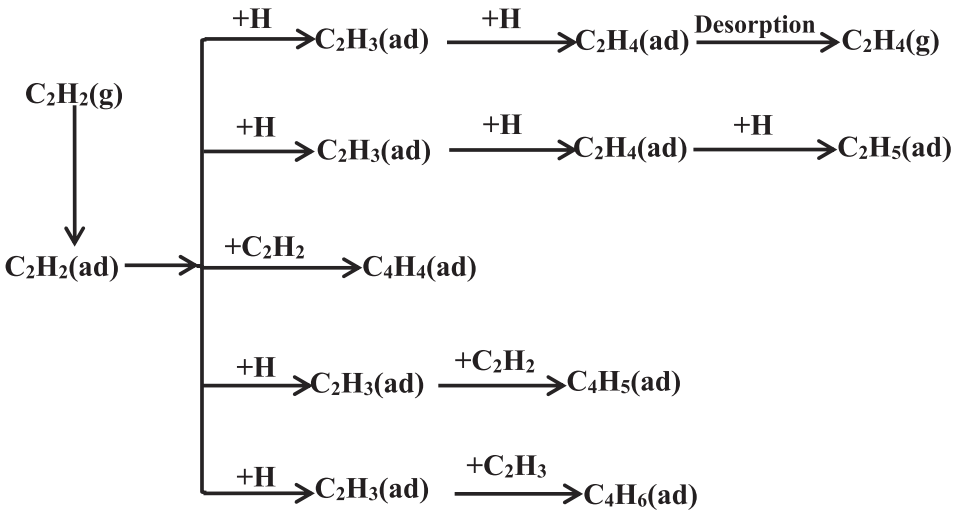

Fig. 2. The possible reaction pathways involving in the selective hydrogenation of C_2H_2 and the formation of 1,3-butadiene; (ad) and (g) stand for the adsorbed and gas phase states, respectively.

Table 1
The adsorption free energies (G_{ads}) of H, C_2H_x(x = 2–5), C_4H_4, C_4H_5 and C_4H_6 species in the selective hydrogenation of C_2H_2 and the formation of 1,3-butadiene over different types of $Cu_2O(1\,1\,1)$ surfaces at 525 K.

Surfaces	G_{ads} (kJ·mol^{-1})							
	H	C_2H_2	C_2H_3	C_2H_4	C_2H_5	C_4H_4	C_4H_5	C_4H_6
Per-$Cu_2O(1\,1\,1)$	202.9	133.4	270.9	116.2	202.1	373.1	278.6	151.6
O_V-$Cu_2O(1\,1\,1)$	255.8	266.7	278.5	145.8	217.4	481.7	308.2	159.9
S_V-$Cu_2O(1\,1\,1)$	225.4	132.1	288.5	110.9	187.1	359.4	298.3	146.6
S_{ad}-$Cu_2O(1\,1\,1)$	237.9	137.9	302.3	141.0	184.0	299.5	284.4	128.1

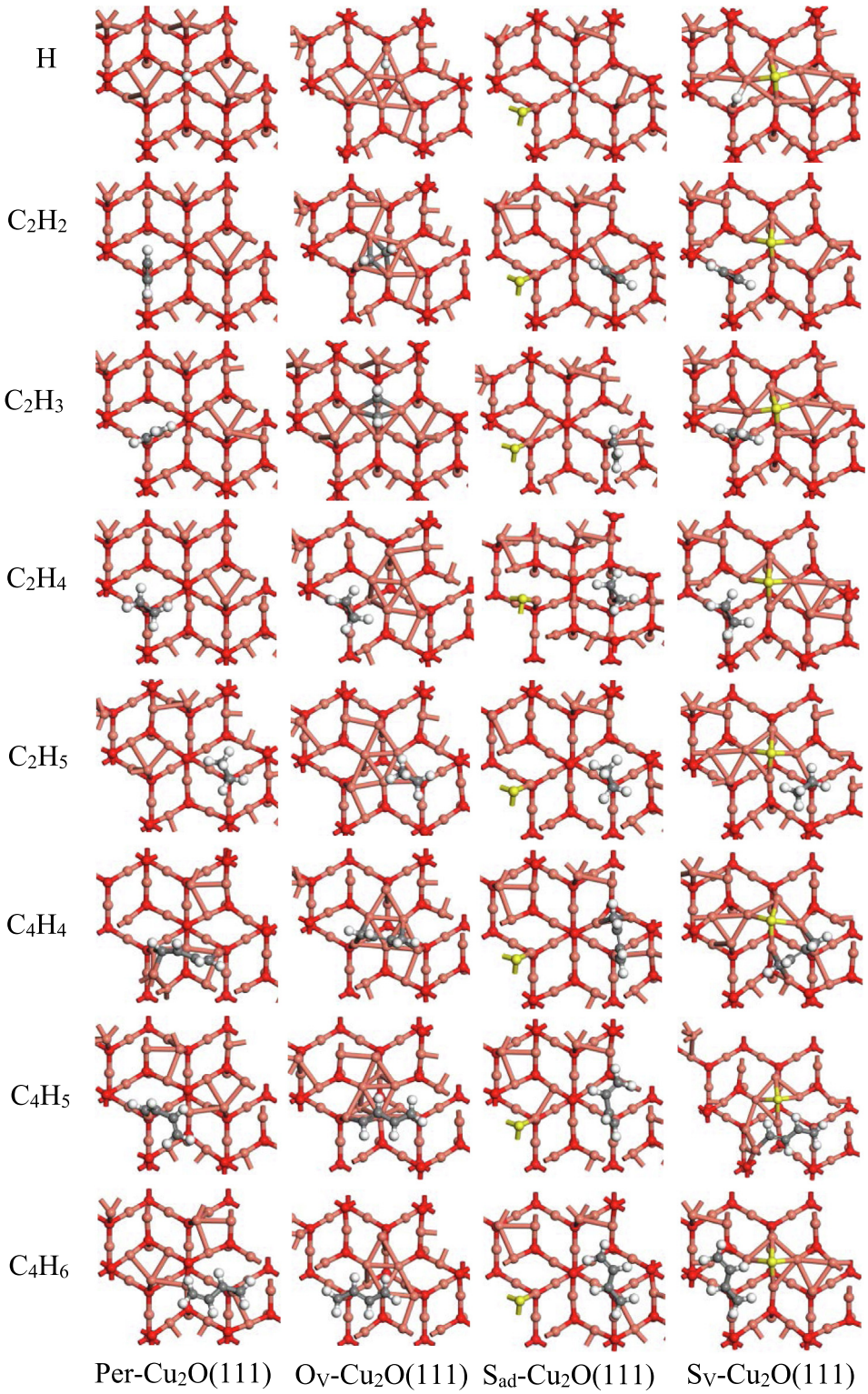

Fig. 3. The most stable adsorption configurations of H, C_2H_2, C_2H_3, C_2H_4, C_2H_5, C_4H_4, C_4H_5 and C_4H_6 species in the selective hydrogenation of C_2H_2 and the formation of 1,3-butadiene over different types of $Cu_2O(1\,1\,1)$ surfaces. C and H atoms are shown in the grey and white balls, respectively.

3. Results and discussion

3.1. The formation of C_2H_4 and 1,3-butadiene

C_2H_2 selective hydrogenation includes the hydrogenation and polymerization processes. Based on previous studies on Cu_2O catalysts (Zhang et al., 2017); ***C_2H_4 intermediate pathway*** to C_2H_6 and ***C_2H_4 desorption pathway*** to gaseous C_2H_4 were considered in the hydrogenation process, as presented in Fig. 2. The energy difference between the activation free energy of C_2H_4 hydrogenation (G_a) and the value of C_2H_4 desorption free energy (G_{des}), ΔG_{sel}, is used as a descriptor to evaluate the selectivity of catalysts toward

Table 2
The activation free energy (G_a) and reaction free energy ($\triangle G$) of all possible elementary reactions involving in the selective hydrogenation of C_2H_2 and the formation of 1,3-butadiene over different types of $Cu_2O(1\,1\,1)$ surfaces at 525 K.

Surfaces	Elementary reaction	G_a/kJ·mol^{-1}	$\triangle G$/kJ·mol^{-1}
Per-Cu_2O(111)	R1-1 $C_2H_2 + H \rightarrow C_2H_3$	87.3	−105.4
	R1-2 $C_2H_3 + H \rightarrow C_2H_4$	104.4	−52.9
	R1-3 $C_2H_4 + H \rightarrow C_2H_5$	85.8	−74.3
	R1-4 $C_2H_2 + C_2H_2 \rightarrow C_4H_4$	139.6	−47.9
	R1-5 $C_2H_3 + C_2H_2 \rightarrow C_4H_5$	284.3	−80.9
	R1-6 $C_2H_3 + C_2H_3 \rightarrow C_4H_6$	247.5	−144.8
O_V-Cu_2O(111)	R2-1 $C_2H_2 + H \rightarrow C_2H_3$	148.6	−35.0
	R2-2 $C_2H_3 + H \rightarrow C_2H_4$	183.1	20.5
	R2-3 $C_2H_4 + H \rightarrow C_2H_5$	171.9	−10.5
	R2-4 $C_2H_2 + C_2H_2 \rightarrow C_4H_4$	136.2	-33.7
	R2-5 $C_2H_3 + C_2H_2 \rightarrow C_4H_5$	263.8	15.4
	R2-6 $C_2H_3 + C_2H_3 \rightarrow C_4H_6$	149.7	−99.5
S_V-Cu_2O(111)	R3-1 $C_2H_2 + H \rightarrow C_2H_3$	35.0	−137.2
	R3-2 $C_2H_3 + H \rightarrow C_2H_4$	87.9	−140.3
	R3-3 $C_2H_4 + H \rightarrow C_2H_5$	146.5	−60.1
	R3-4 $C_2H_2 + C_2H_2 \rightarrow C_4H_4$	275.6	-22.9
	R3-5 $C_2H_3 + C_2H_2 \rightarrow C_4H_5$	167.0	−133.2
	R3-6 $C_2H_3 + C_2H_3 \rightarrow C_4H_6$	277.7	−147.9
S_{ad}-Cu_2O(111)	R4-1 $C_2H_2 + H \rightarrow C_2H_3$	142.9	−54.3
	R4-2 $C_2H_3 + H \rightarrow C_2H_4$	112.0	−57.4
	R4-3 $C_2H_4 + H \rightarrow C_2H_5$	148.7	−16.1
	R4-4 $C_2H_2 + C_2H_2 \rightarrow C_4H_4$	220.0	−26.4
	R4-5 $C_2H_3 + C_2H_2 \rightarrow C_4H_5$	282.3	−92.4
	R4-6 $C_2H_3 + C_2H_3 \rightarrow C_4H_6$	238.2	−150.6

C_2H_4 formation (Yang et al., 2012; Sheth et al., 2005), as presented in Eq. (1):

$$\Delta G_{sel} = G_a - G_{des} \quad (1)$$

Where the more positive ΔG_{sel} is, the better the selectivity of C_2H_4 formation is.

In the polymerization process, 1,3-butadiene can be formed via the hydrogenation-coupling or coupling-hydrogenation pathways (Sarkany et al., 1984). Thus, as shown in Fig. 2, three pathways, $C_2H_2 + C_2H_2$, $C_2H_2 + C_2H_3$ and $C_2H_3 + C_2H_3$, were examined, which leads to C_4H_x formation and eventually followed by its hydrogenation to 1,3-butadiene.

For the H, C_2H_x($x = 2 \sim 5$), C_4H_4, C_4H_5 and C_4H_6 species involving in the hydrogenation and polymerization processes of C_2H_2, the adsorption free energies at 525 K and the most stable adsorption configurations over different types of $Cu_2O(1\,1\,1)$ surfaces are shown in Table 1 and Fig. 3, respectively. Meanwhile, the activation free energy and free reaction energy of possible elementary reactions are listed in Table 2.

3.2. Formation of C_2H_4 and 1,3-butadiene on the surfaces of sulfur-free Cu_2O

3.2.1. Perfect $Cu_2O(1\,1\,1)$ surface

For the hydrogenation process of C_2H_2 (Fig. 4), the hydrogenation activation free energy and desorption free energy of adsorbed C_2H_4 are 85.8 and 116.2 kJ·mol^{-1}, respectively. The ΔG_{sel} is −30.4 kJ·mol^{-1}, suggesting that the over-hydrogenation of C_2H_4 to ethane easily occurs compared to C_2H_4 desorption pathway to gaseous C_2H_4. As a result, ethane is the dominant product instead of C_2H_4.

For 1,3-butadiene formation, as presented in Fig. 4, $C_2H_2 + C_2H_2$ pathway only includes one elementary reaction of $C_2H_2 + C_2H_2 \rightarrow C_4H_4$ with the activation free energy of 139.6 kJ·mol^{-1}; $C_2H_2 + C_2H_3$ pathway includes two elementary reactions of $C_2H_2 + H \rightarrow C_2H_3$ and $C_2H_2 + C_2H_3 \rightarrow C_4H_5$; similarly, $C_2H_3 + C_2H_3$ pathway includes two elementary reactions of $C_2H_2 + H \rightarrow C_2H_3$ and $C_2H_3 + C_2H_3 \rightarrow C_4H_6$. Thus, starting from C_2H_2 species, the $C_2H_2 + C_2H_3$ and $C_2H_3 + C_2H_3$ pathways have the overall activation free energies of 178.9 and 142.1 kJ·mol^{-1}, respectively. As a result, the pathways of $C_2H_2 + C_2H_2$ and $C_2H_3 + C_2H_3$ are more favorable kinetically than $C_2H_2 + C_2H_3$ pathway.

As mentioned above, ethane is the major product for the hydrogenation process of C_2H_2. Obviously, the activation free energy of rate-controlling step (104.4 kJ·mol^{-1}) and the overall activation free energies (87.3 kJ·mol^{-1}) for the most favorable formation pathway of ethane are smaller than those (139.6 and 139.6 kJ·mol^{-1} for $C_2H_2 + C_2H_2$ pathway, 142.1 and 142.1 kJ·mol^{-1} for $C_2H_3 + C_2H_3$ pathway) of 1,3-butadiene formation. Thus, C_2H_2 over-hydrogenation to ethane is more favorable than C_2H_2 coupling to 1,3-butadiene, the perfect $Cu_2O(1\,1\,1)$ surface can effectively reduce the formation possibility of green oil; however, it can catalyze C_2H_2 over-hydrogenation to ethane.

3.2.2. Oxygen-vacancy $Cu_2O(1\,1\,1)$ surface

As shown in Fig. 5, C_2H_4 hydrogenation activation and desorption free energies of C_2H_4 are 171.9 and 145.8 kJ·mol^{-1}, respectively. The corresponding ΔG_{sel} is 26.1 kJ·mol^{-1}, namely, C_2H_4 desorption from catalyst surface is more preferred than its hydrogenation, C_2H_4 is the major product on the oxygen-vacancy Cu_2O (1 1 1) surface with the overall activation free energies of 148.6 kJ·mol^{-1}; the rate-controlling step for this reaction ($C_2H_3 + H \rightarrow C_2H_4$) has an activation free energy of 183.1 kJ·mol^{-1}. For 1,3-butadiene formation, starting from C_2H_2 species, the overall activation free energies of $C_2H_2 + C_2H_2$, $C_2H_2 + C_2H_3$ and $C_2H_3 + C_2H_3$ pathways are 136.2, 228.8 and 148.6 kJ·mol^{-1}, respectively; meanwhile, the rate-controlling steps of $C_2H_2 + C_2H_2$ and $C_2H_3 + C_2H_3$ pathways have activation free energies of 136.2 and 149.7 kJ·mol^{-1}, respectively. Thus, the pathway of $C_2H_2 + C_2H_2$ is the most favorable for the formation of 1,3-butadiene.

As mentioned above, compared to the most favorable pathway of C_2H_4 formation (183.1 and 148.6 kJ·mol^{-1}), the activation free energy of rate-controlling step and the overall activation free energy for the most favorable pathway of 1,3-butadiene formation (136.2 and 136.2 kJ·mol^{-1}) is more favorable, suggesting that the oxygen-vacancy $Cu_2O(1\,1\,1)$ surface exhibits good C_2H_4 selectivity; however, the formation of green oil precursor easily occurred.

3.3. Formation of C_2H_4 and 1,3-butadiene on the surfaces of sulfur-containing Cu_2O

3.3.1. Sulfurized $Cu_2O(1\,1\,1)$ surface

As shown in Fig. 6, the hydrogenation activation and desorption free energies of adsorbed C_2H_4 are 146.5 and 110.9 kJ·mol^{-1}, respectively, and the corresponding ΔG_{sel} is 35.6 kJ·mol^{-1}, suggesting that C_2H_4 prefers to desorb rather than being hydrogenated, and the sulfurized $Cu_2O(1\,1\,1)$ surface exhibits good selectivity toward C_2H_4 formation instead of ethane formation. The rate-controlling step is C_2H_4 desorption with an activation free energy of 110.9 kJ·mol^{-1}.

For 1,3-butadiene formation, starting from C_2H_2 species, the overall activation free energies of $C_2H_2 + C_2H_2$, $C_2H_2 + C_2H_3$ and $C_2H_3 + C_2H_3$ pathways are 275.6, 35.0 and 140.5 kJ·mol^{-1}, respectively, indicating that $C_2H_2 + C_2H_3$ pathway is the most favorable kinetically (35.0 kJ·mol^{-1}), correspondingly, the activation free energy of rate-controlling step $C_2H_2 + C_2H_3 \rightarrow C_4H_5$ is 167.0 kJ·mol^{-1}.

The comparisons of the most favorable pathway between C_2H_4 and 1,3-butadiene formation shows that starting from C_2H_2 species, the overall activation free energies of C_2H_4 and 1,3-butadiene formation are the same (35.0 kJ·mol^{-1}), both pathways go through the common intermediate C_2H_3, however, the activation free energies of $C_2H_3 + H$ is much lower than that of $C_2H_3 + C_2H_2$ (87.9 *vs* 167.0 kJ·mol^{-1}), namely, the hydrogenation

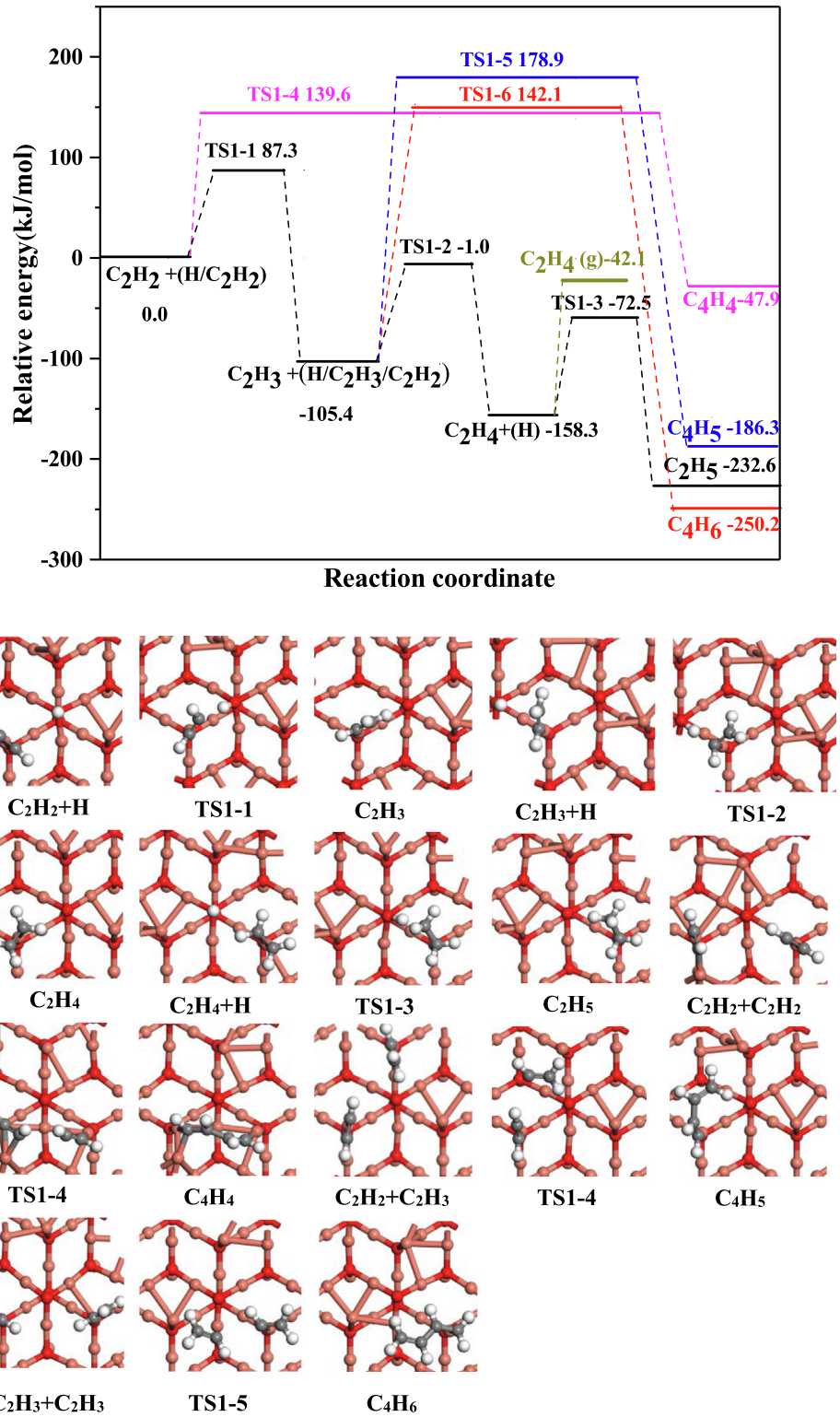

Fig. 4. Energy profiles for the pathways involving in the selective hydrogenation of C_2H_2 and the formation of 1,3-butadiene together with the structures of initial states, transition states and final states on the perfect $Cu_2O(111)$ surface at 525 K.

pathway to form C_2H_4 is kinetically favored than the polymerization pathway of C_2H_3 + C_2H_2 to form 1,3-butadiene. Thus, the sulfurized $Cu_2O(1\,1\,1)$ surface possess not only high selectivity toward C_2H_2 hydrogenation to gaseous C_2H_4, but also good ability to reduce the formation of green oil precursor. Consequently, the sulfurized $Cu_2O(1\,1\,1)$ surface can be used as an excellent catalyst in C_2H_2 selective hydrogenation.

3.3.2. Pre-sulfur-adsorbed sulfur $Cu_2O(1\,1\,1)$ surface

As presented in Fig. 7, the activation free energy of C_2H_4 hydrogenation and its desorption free energy are 148.7 and 141.0 kJ·mol^{-1}, respectively. Thus, a ΔG_{sel} of 7.7 kJ·mol^{-1} suggests that C_2H_4 desorption is slightly more favorable than its hydrogenation. C_2H_4 is the main product on the pre-adsorbed sulfur Cu_2O $(1\,1\,1)$ surface.

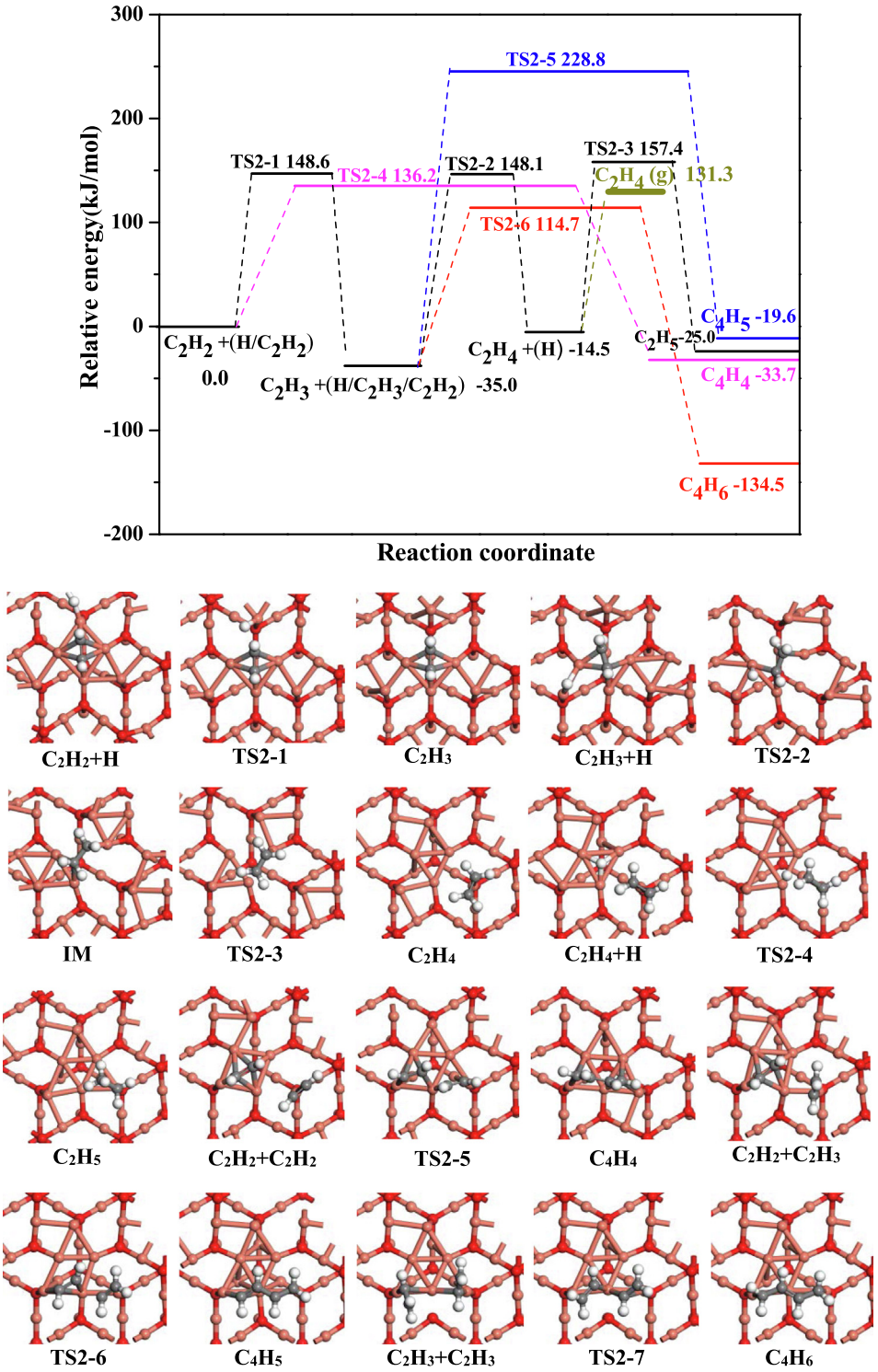

Fig. 5. Energy profiles for the pathways involving in the selective hydrogenation of C_2H_2 and the formation of 1,3-butadiene together with the structures of initial states, transition states and final states on the oxygen-vacancy $Cu_2O(111)$ surface at 525 K.

For 1,3-butadiene formation, the overall activation free energies of C_2H_2 + C_2H_2, C_2H_2 + C_2H_3 and C_2H_3 + C_2H_3 pathways are 222.0, 228.0 and 183.9 kJ·mol^{-1}, respectively. Thus, the pathway of C_2H_3 + C_2H_3 is the most favorable, the activation free energy of the rate-controlling step $C_2H_3 + C_2H_3 \rightarrow C_4H_6$ for 1,3-butadiene formation is 238.2 kJ·mol^{-1}.

Comparing the most favorable pathway of C_2H_4 formation with that of 1,3-butadiene, the overall activation free energy of C_2H_4 formation (142.9 kJ·mol^{-1}) is lower than that of 1,3-butadiene formation (183.9 kJ·mol^{-1}). Moreover, the activation free energy of the rate-controlling step for 1,3-butadiene formation (238.2 kJ·mol^{-1}) is larger than that for C_2H_4 formation (142.9 kJ·mol^{-1}). Thus, C_2H_2 prefers to be hydrogenated for the generation of C_2H_4 instead of 1,3-butadiene on the pre-sulfur-adsorbed $Cu_2O(111)$. Namely, the pre-sulfur-adsorbed Cu_2O (111) surface also presents good selectivity toward C_2H_2 hydrogenation to C_2H_4 and good ability to reduce green oil precursor formation.

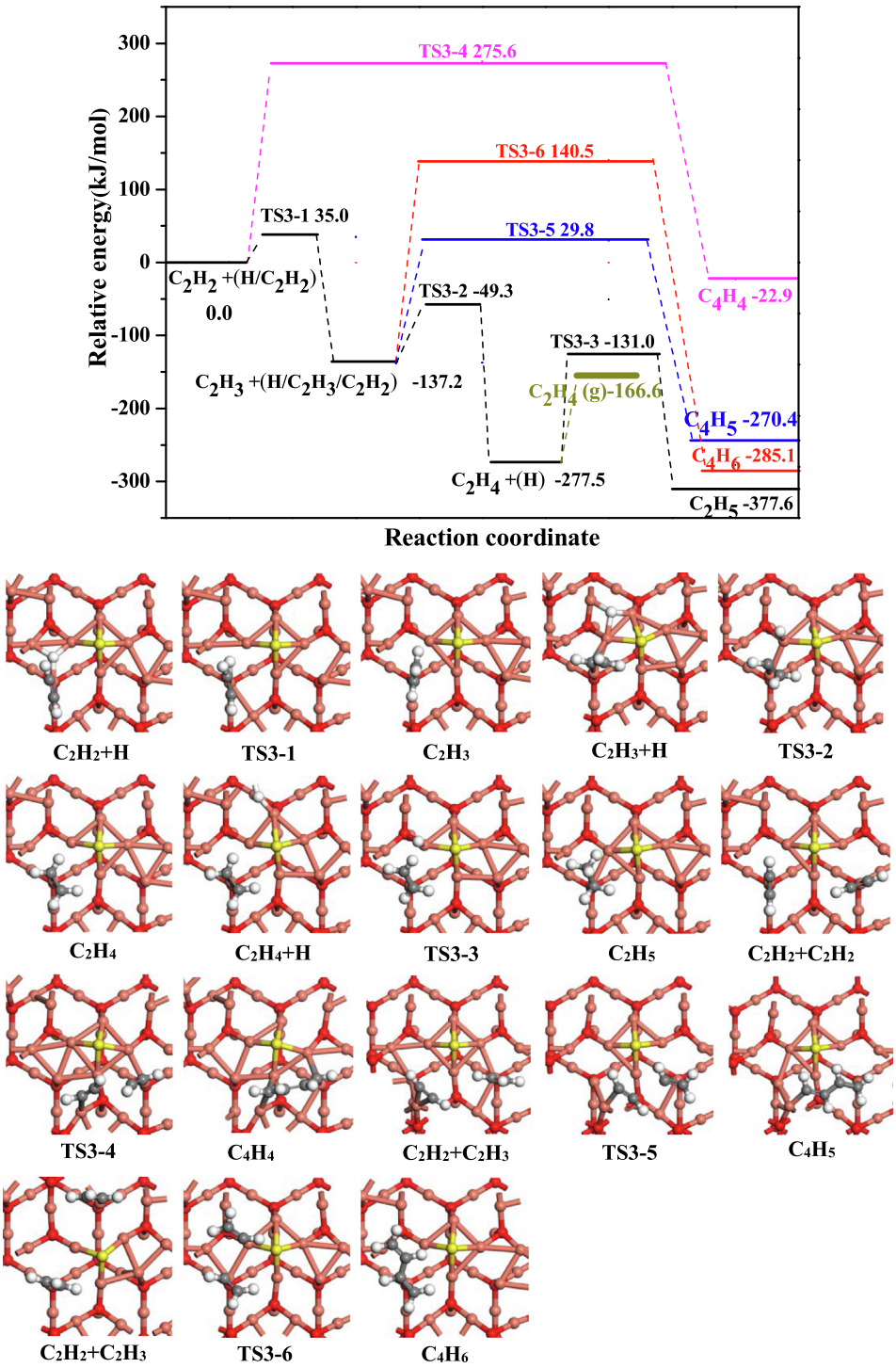

Fig. 6. Energy profiles for the pathways involving in the selective hydrogenation of C_2H_2 and the formation of 1,3-butadiene together with the structures of initial states, transition states and final states on the sulfurized $Cu_2O(111)$ surface at 525 K.

Above results showed that the favorable pathways of the dimerization to 1,3-butadiene on the perfect, oxygen-vacancy, sulfurized and pre-adsorbed sulfur $Cu_2O(111)$ are different, which may depend on the types of used catalysts. For example, Zhao *et al.* (Zhao et al., 2019) explored green oil formation on the (111) surface of Ag, Cu, Pd, Pt, Rh and Ir catalysts, the dimerization of C_2H_3 + C_2H_3 was the most favorable on the Ag (111) and Cu(111), which is similar to that on the pre-adsorbed sulfur $Cu_2O(111)$; the dimerization of C_2H_3 + C_2H_3 or C_2H_2 on Rh(111) are favored to form green oil, which is similar to that on the perfect $Cu_2O(111)$; the dimerization of C_2H_2 + C_2H_3 was the most favorable on the Pd(111), Pt(111) and Ir(111); Meanwhile, García-Mota *et al.* (García-Mota et al., 2010) also suggested that the dimerization of C_2H_2 + C_2H_3 was also preferred on Pd(111) to form green oil, which is similar to that on the sulfurized $Cu_2O(111)$. These catalysts have nothing in common for the pathway of the involvement of partially hydrogenated species, thus, the differences of the most favorable pathway for the dimerization may be attributed to the different surface electronic properties.

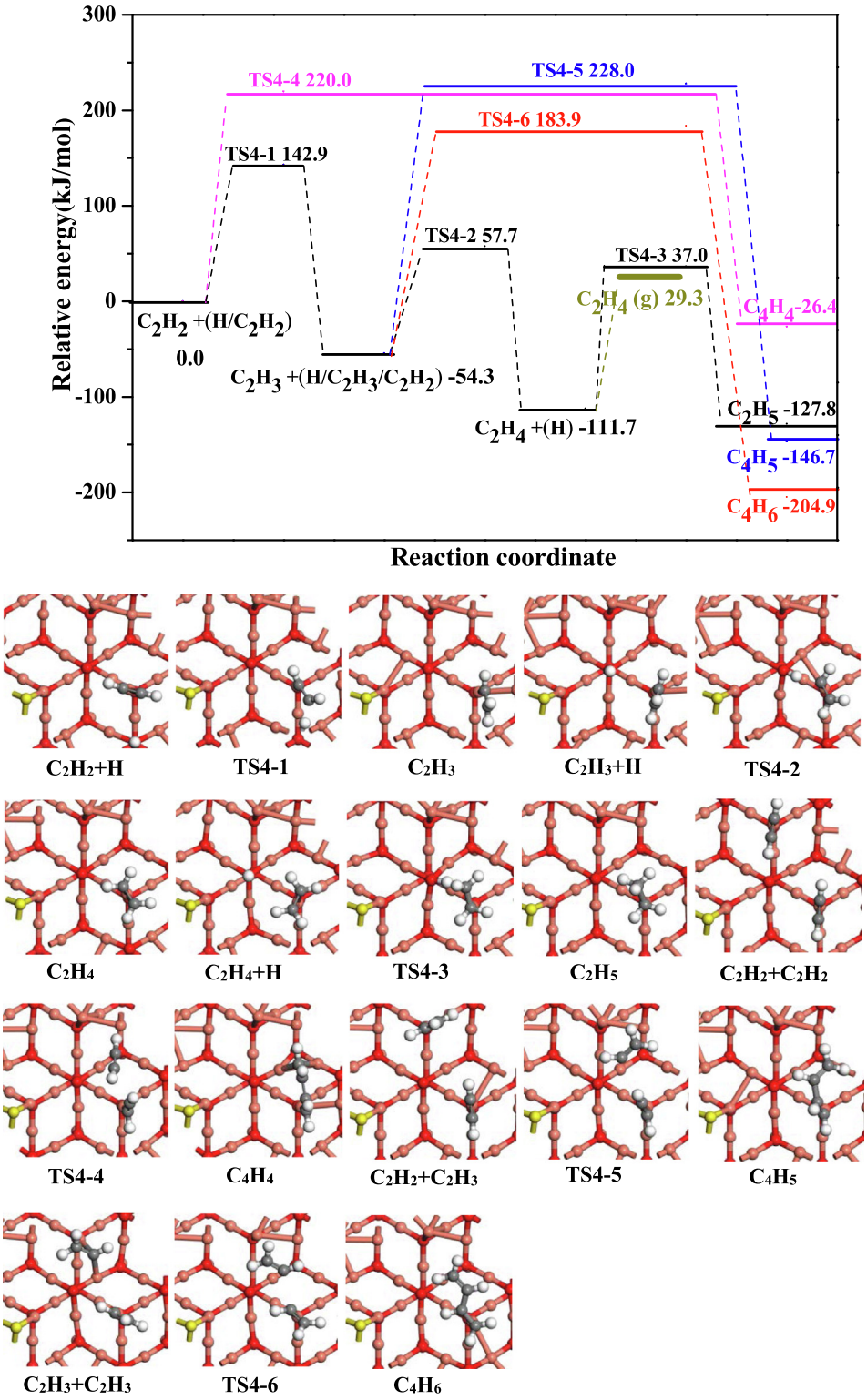

Fig. 7. Energy profiles for the pathways involving in the selective hydrogenation of C_2H_2 and the formation of 1,3-butadiene together with the structures of initial states, transition states and final states on the pre-adsorbed sulfur $Cu_2O(111)$ surface at 525 K.

3.4. General discussion

3.4.1. The effect of the S on C_2H_4 selectivity and green oil precursor formation

Evidently, the surface morphologies of sulfur-free Cu_2O affect the favorability of the pathway for C_2H_2 hydrogenation and coupling reactions, as presented in Fig. 8. On the perfect $Cu_2O(111)$, the most favorable pathways of the hydrogenation and polymerization processes correspond to C_2H_4 intermediate pathway to ethane and C_2H_2 + C_2H_2 (C_2H_3 + C_2H_3) to C_4H_4 (C_4H_6), respectively, namely, ethane formation is kinetically more favored than C_4H_4 (C_4H_6) formation, thus, the perfect $Cu_2O(111)$ surface is able to reduce green oil formation, while it is poor in catalyzing C_2H_4 formation. On the oxygen-vacancy $Cu_2O(111)$, the most favorable pathways of the hydrogenation and polymerization processes correspond to C_2H_4 desorption pathway and C_2H_2 + C_2H_2 to C_4H_4,

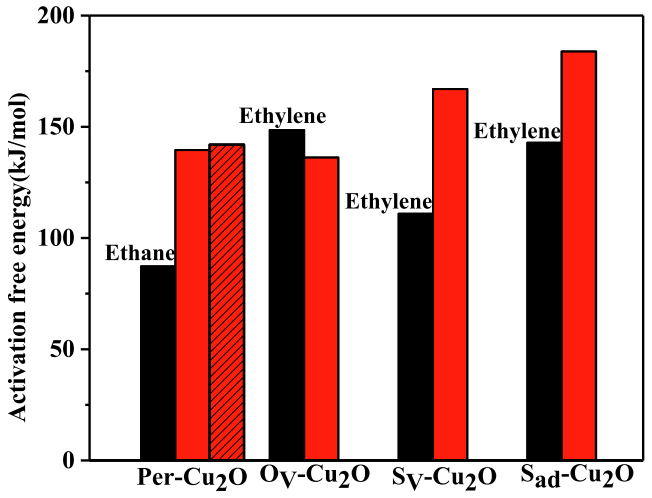

Fig. 8. Comparisons about the overall activation free energy between ethylene (ethane) and 1,3-butadiene formation on the Per-$Cu_2O(111)$, O_V-$Cu_2O(111)$, S_V-$Cu_2O(111)$ and S_{ad}-$Cu_2O(111)$ surfaces. (The activation free energy of rate-controlling step for gaseous C_2H_4 and 1,3-butadiene formation are used on S_V-$Cu_2O(111)$ surface due to the same overall activation free energy). The black bars represent ethylene (ethane) formation, the red bars represent 1,3-butadiene formation. (For interpretation of the references to colour in this figure legend, the reader is referred to the web version of this article.)

respectively; C_4H_4 formation is kinetically more favored than C_2H_4 desorption from the surface, thus, the oxygen-vacancy $Cu_2O(111)$ exhibits high selectivity toward C_2H_2 hydrogenation to gaseous C_2H_4, whereas it presents poor ability to reduce green oil formation.

Sulfur-containing Cu_2O catalysts behave differently. On the sulfurized $Cu_2O(111)$, C_2H_4 desorption and C_2H_2 + C_2H_3 pathways are advantageous to C_2H_2 hydrogenation and coupling reactions, and thus the formations of gaseous C_2H_4 and 1,3-butadiene, respectively. However, gaseous C_2H_4 formation is more favored kinetically than C_4H_5 formation, thus, C_2H_4 formation is much easier, namely, the sulfurized $Cu_2O(111)$ surface is capable of not only reducing green oil formation but also leading to high C_2H_4 selectivity. On the pre-sulfur-adsorbed $Cu_2O(111)$, the most favorable pathways of the hydrogenation and polymerization processes correspond to C_2H_4 desorption to gaseous C_2H_4 and C_2H_3 + C_2H_3 to C_4H_6, respectively, obviously, gaseous C_2H_4 formation is kinetically more favored than C_4H_6 formation; thus, the pre-sulfur-adsorbed $Cu_2O(111)$ is good at reducing green oil formation and strong in C_2H_2 hydrogenation to C_2H_4.

As mentioned above, the sulfur-free Cu_2O catalysts are not good candidates for the selective hydrogenation of C_2H_2 due to the low selectivity of perfect $Cu_2O(111)$ surface toward C_2H_4 formation and the poor ability of oxygen-vacancy $Cu_2O(111)$ surface in reducing green oil formation. However, the sulfur-containing Cu_2O catalysts including the sulfurized and pre-sulfur-adsorbed $Cu_2O(111)$ surfaces perform well in both selective hydrogenation of C_2H_2 to C_2H_4 and reduce green oil generation.

3.4.2. The effect of the S on the activity of C_2H_4 formation

As presented in Table 3, to describe quantitatively the catalytic activity of different types of Cu_2O catalysts in C_2H_2 hydrogenation to C_2H_4, the two-step model reported by Hu *et al.* (Cheng et al., 2008; Cheng and Hu, 2011) (see details in the Supplementary Material) was used. The model was used for calculating the reaction rates with the coverage terms of all the associated species during C_2H_2 hydrogenation; the reaction rates (s^{-1}·site^{-1}) of C_2H_4 formation on Cu_2O catalyst follow the order of S_V-$Cu_2O(111)$ (3.09×10^9) > Per-$Cu_2O(111)$ (2.25×10^4) > S_{ad}-$Cu_2O(111)$ (6.62×10^{-2}) > O_V-$Cu_2O(111)$ (1.79×10^{-2}).

On the other hand, the catalytic performance of Cu_2O is compared with that of the conventional Pd surfaces. Firstly, Yang *et al.* (Yang et al., 2013) calculated C_2H_4 selectivity and its formation activity on the Pd(111), Pd(100), Pd(211) and Pd(211)-defect surfaces, suggesting that only Pd(111) has relatively good C_2H_4 selectivity, the values of C_2H_4 selectivity on theses surfaces are 5.79, −28.95, −43.42 and −36.66 kJ·mol^{-1}, respectively; the values of effective barriers (*G*de P) for C_2H_2 hydrogenation on these surfaces are 103.24, 129.29, 93.59 and 104.2 kJ·mol^{-1}, respectively. Zhao *et al.* (Zhao et al., 2019) calculated the priority of C_2 hydrogenation and C_2 coupling in C_2H_2 hydrogenation on Pd(111), C_2 hydrogenation pathway is slightly better than C_2 coupling pathway (97.45 and 99.38 kJ·mol^{-1}). Thus, compared to above studies on Pd catalyst, S_v-$Cu_2O(111)$ catalyst in our study exhibits better activity and selectivity toward gaseous C_2H_4 formation, the values of C_2H_4 selectivity and *G*de P on S_v-$Cu_2O(111)$ are 35.6 and 35.0 kJ·mol^{-1}, respectively; Meanwhile, the activation free energies of C_2 hydrogenation and C_2 coupling are 87.9 and 167.0 kJ·mol^{-1}, respectively, S_v-$Cu_2O(111)$ can effectively reduce green oil formation.

To further illustrate the reason why the sulfur-containing Cu_2O catalysts can improve the catalytic activity of gaseous C_2H_4 formation, the surface structure characteristics of different types of Cu_2O surfaces are examined. As shown in Fig. 4, the Cu_{CUS} sites are the active sites for the hydrogenation of C_2H_2, when the catalyst active sites are affected, its corresponding catalytic activity changes, such as the oxygen-vacancy on O_v-$Cu_2O(111)$ and the pre-adsorbed S on S_{ad}-$Cu_2O(111)$ change the coordination unsaturation of Cu_{CUS} and reduce the numbers of Cu_{CUS} active site, therefore decrease the catalytic activity of Cu_2O catalysts, which might be the reason why the S_{ad}-$Cu_2O(111)$ and O_V-$Cu_2O(111)$ surfaces have lower catalytic activity than the perfect $Cu_2O(111)$ surface. On the other hand, as shown in Fig. 6, the sulfur atom change the adsorption site of H atoms on S_V-$Cu_2O(111)$, which make C_2H_2 and H adsorbed at the Cu_{CUS} site and Cu_{CSA}-Cu_{CSA} bridge, respectively. Clearly, the co-adsorption of H and C_2H_2 is much closer compared to that over the perfect surface, which is in favor of C_2H_2 hydrogenation to C_2H_4. As a result, S_V-$Cu_2O(111)$ surface has the higher catalytic activity than the perfect $Cu_2O(111)$ surface.

3.4.3. The analysis of electronic properties

In order to further clarify the effect of S on Cu_2O catalysts during the hydrogenation to C_2H_4, the *d*-band center for the S-free and S-containing Cu_2O catalysts was calculated. Among four types of catalysts, the *d*-band centers (eV) for O_V-$Cu_2O(111)$ (-1.808) and Per-$Cu_2O(111)$ (-1.810) are closer to the Fermi energy level; whereas

Table 3
Hydrogenation activation free energy (G_a/kJ·mol^{-1}) and the adsorption free energy (G_{ads}/kJ·mol^{-1}) of C_2H_4, as well as the energy differences (ΔG_{sel}/kJ·mol^{-1}) between G_a and G_{des}, the reaction rate (r/s^{-1}·site^{-1}) involving in the selective hydrogenation of C_2H_2 on different types of $Cu_2O(111)$ surfaces at 525 K.

Surfaces	G_a	G_{ads}	ΔG_{sel}	$G^{ad}{}_R$-$G^{de}{}_R$ + $G^{de}{}_P$	$G^{de}{}_P$	r
Per-$Cu_2O(111)$	85.8	116.2	−30.4	−54.7	87.3	2.25×10^4
O_V-$Cu_2O(111)$	171.9	145.8	26.1	−166.8	148.6	1.79×10^{-2}
S_V-$Cu_2O(111)$	146.5	110.9	35.6	17.5	35.0	3.09×10^9
S_{ad}-$Cu_2O(111)$	148.7	141.0	7.7	−70.5	142.9	6.62×10^{-2}

the *d*-band centers for S_V-Cu_2O(111) (-1.819) and S_{ad}-Cu_2O(111) (-2.103) are more away from the Fermi energy level. Namely, the distance from the *d*-band center to the Fermi energy level is too close, which would lead to ethane or green oil formation, whereas it would lead to high selectivity of C_2H_4 formation and reduce ethane and green oil formation; meanwhile, the distance between the *d*-band center and the Fermi energy level should be kept within a moderate range in order to achieve high catalytic activity for C_2H_2 hydrogenation to C_2H_4 over the S-containing Cu_2O catalysts.

Zhang *et al.* (Zhang et al., 2018) investigated C_2H_2 hydrogenation on the NiCu(111), AuCu(111), PtCu(111), PdCu(111), Cu(111) and Pd(111) with the distance between *d*-band center and Fermi energy of −2.32, −2.67, −2.49, −2.45, −2.47 and −2.02 eV, respectively, and C_2H_4 selectivity and its formation activity has a roughly volcano type relationship with the location of surface *d*-band centers, PdCu(111) exhibits the highest C_2H_4 selectivity and formation activity with a moderate location of *d*-band center (-2.45 eV). Zhang et al., 2018 explored C_2H_2 hydrogenation on the AgCu(211), PtCu(211), PdCu(211), RhCu(211) and NiCu(211) with the distance between *d*-band center and Fermi energy of −2.67, −2.32, −2.28, −2.18 and −2.14 eV, respectively, suggesting that the location of *d*-band center has a roughly volcano type relationship with C_2H_4 selectivity and its formation activity, PdCu(211) with the moderate location of *d*-band center (-2.28 eV) exhibits the best C_2H_4 selectivity and formation activity. Further, Wang *et al.* (Wang et al., 2021) investigated C_2H_2 hydrogenation on the Pd intermetallic catalyst, the distance between *d*-band center and Fermi energy for the $PdAg_3$(111), PdAg(111) and Pd_3Ag(111) are −3.14, −2.46 and −2.14 eV, respectively, in which PdAg(111) with the moderate location of *d*-band center (-2.46 eV) not only reduce green oil formation, but also exhibit better C_2H_4 selectivity and its formation activity. Above results show that the catalysts with a moderate *d*-band center exhibit better catalytic performance toward C_2H_2 hydrogenation, in which the moderate range of *d*-band center depends on the types of catalysts.

3.4.4. The microscopic mechanism toward the desired performance of S-containing Cu_2O catalysts

To explore the mechanism of the great performance of H_2S or S-containing Cu_2O catalysts during C_2H_2 hydrogenation, all adsorption configuration of the initial states and their coupling reactions in Figs. 4 ~ 7 were examined over four types of Cu_2O(111) surfaces. Fig. 9 presents the effect of S on the formation of C_2H_4, C_2H_6 and green oil precursor over the S-free and S-containing Cu_2O catalysts. The S_V-Cu_2O(111) and O_V-Cu_2O(111) surfaces with high C_2H_4 selectivity are used for illustrating the role of surface S over Cu_2O catalysts.

During C_2H_2 hydrogenation, both C_2H_2 and H on the sulfur-containing Cu_2O catalysts are adsorbed at the Cu_{CUS} and Cu_{CSA}-Cu_{CSA} bridge sites, respectively. As indicated, the interaction of H with C_2H_2 is in one hexagon region, which makes C_2H_2 hydrogenation to C_2H_4 occur more easily. However, on the sulfur-free Cu_2O, both C_2H_2 and H are adsorbed at the Cu_{CUS} and oxygen-vacancy sites, respectively. Here, the interaction of H with C_2H_2 in two adjacent hexagon regions is not in favor of C_2H_2 hydrogenation to C_2H_3 and then to C_2H_4. Thus, the S atoms make the interaction distance between H and C_2H_2 (C_2H_3) closer over Cu_2O catalysts to promote C_2H_2 hydrogenation to C_2H_4 in one hexagon region.

How does C_2H_4 hydrogenation occur on the sulfur-free Cu_2O catalysts? C_2H_4 and H are adsorbed at the Cu_{CUS} and oxygen-vacancy sites in one hexagon region. However, on the sulfur-containing Cu_2O catalysts, both C_2H_4 and H are adsorbed at the

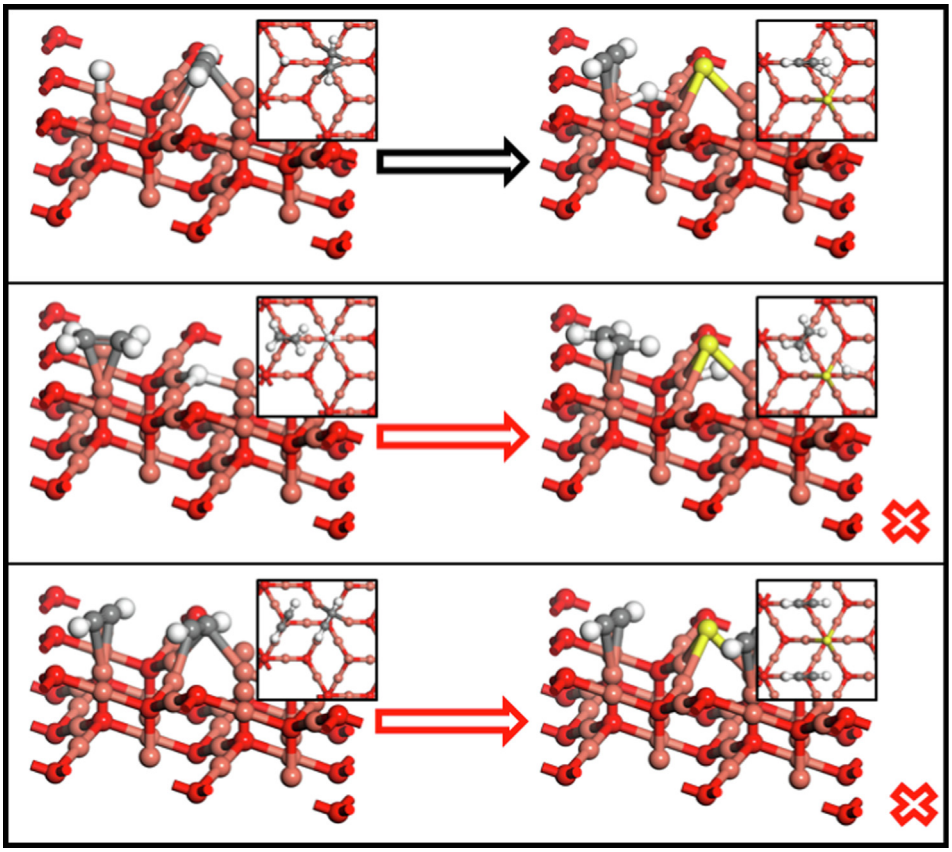

Fig. 9. The sketch map for the effect of surface S on the formation of ethylene, ethane and green oil precursor over the sulfur-free and sulfur-containing Cu_2O catalysts. (For interpretation of the references to colour in this figure legend, the reader is referred to the web version of this article.)

Cu_{CUS} and Cu_{CSA}-Cu_{CSA} bridge sites in two adjacent hexagon regions, as such, the S atoms make the interaction distance of H and C_2H_4 longer, which is not in favor of C_2H_4 hydrogenation. As a result, C_2H_4 on the sulfur-containing Cu_2O catalysts is easier to desorb from the catalyst surface and increases the probability of C_2H_4 formation.

How does C_2H_2 coupling occur on the sulfur-free Cu_2O catalysts? They are adsorbed at the Cu_{CUS} and oxygen-vacancy sites in one hexagon region, respectively. However, on the sulfur-containing Cu_2O catalysts, two C_2H_2 are adsorbed at two Cu_{CUS} sites in two adjacent hexagon regions, suggesting that the S atoms make the interaction distance of two C_2H_2 longer, which does not favor C_2H_2 coupling. The same interaction logic applies in the coupling reaction of C_2H_3 + C_2H_2 and C_2H_3 + C_2H_2. Therefore, the sulfur-containing Cu_2O catalysts are beneficial to the reduction of green oil precursor.

In summary, based on above analysis, it is concluded that for the formation reaction of C_2H_4 and green oil, the surface S atom modifies the surface morphology of Cu_2O catalyst, and changes the spatial scale of active region required for the reactions, and therefore it alters the interaction ability of reactants to form the products, specifically, the surface S atom blocked the larger spatial active sites required for the polymerization of C_2H_2 to generate green oil and C_2H_4 hydrogenation to ethane, whereas the surface S atom cannot affect C_2H_2 hydrogenation to C_2H_4 reactions, since these reactions only need smaller spatial active sites. In addition, in our next work, we will quantitatively measure the size of the space scale of the active region to exhibit the most appropriate catalytic performance, and provide an experimental clue for the coverage of S over Cu_2O catalysts.

4. Conclusions

Sulfur, a typical catalyst poison, was found to be a promising candidate for not only enhancing C_2H_4 selectivity but also reducing the generation of 1,3-butadiene as the precursor of green oil during C_2H_2 hydrogenation. Realization of multiple purposes with S in this field is paramount, especially considering the fact that sulfur is often present in form of H_2S as a contaminant in the feeding stream during C_2H_4 production. However, more works need to be conducted prior to the theoretical and technological matures in the uncharted S-containing catalyst development for cost-effective production of C_2H_4, the most important monomer for organic synthesis. These include further understanding the role of subsurface atoms in the formation of effective and stable transition states and quantifying the need of S and optimizing the associated reaction conditions during the important catalytic hydrogenation process.

Declaration of Competing Interest

The authors declare that they have no known competing financial interests or personal relationships that could have appeared to influence the work reported in this paper.

Acknowledgment

This work is financially supported by the National Natural Science Foundation of China (No. 22078221, 21776193), the China Scholarship Council (201606935026).

Appendix A. Supplementary data

Supplementary data to this article can be found online at https://doi.org/10.1016/j.ces.2021.116984.

References

Zhong, X.H., 2011. The study of acetylene selective hydrogenation activity on Cu/SiO2 catalysts. Ms. D. Thesis, Dalian University of Technology.
J. S. Beck, W. O. Haag, F. Buonomo, D. Sanfilippo, F. Trifirò, H. Arnold, F. Döbert, J. Gaube, Handbook of heterogeneous catalysis; VCH: Germany. Vol. 5 (2008) p2165.
True, W.R., 2013. Global ethylene capacity poised for major expansion. Oil Gas J. 111, 90–94.
Magyar, S., Hanesok, J., Kallo, D., 2005. Hydrodesulfurization and hydroconversion of heavy FCC gasoline on PtPd/H-USY zeolite. Fuel Process. Technol. 86, 115l–1164.
Liu, M.J., Deng, Q.G., Zhao, F.J., 2012. Origin of hydrogen sulfide in coal seams in china. Surf. Sci. 50, 668–673.
Williams, B., 2003. Refiners' future survival hinges on updating to changing feedstocks, product specs. Oil Gas J. 101, 20–34.
Borodziński, A., Bond, G.C., 2006. Selective hydrogenation of ethyne in ethene-rich streams on palladium catalysts, Part 1: Effect of changes to the catalyst during reaction. Cat. Rev. - Sci. Eng. 48, 91–144.
Borodziński, A., Bond, G.C., 2008. Selective hydrogenation of ethyne in ethene-rich streams on palladium catalysts, Part 2: Steady-state kinetics and effects of palladium particle size, carbon monoxide, and promoters. Cat. Rev. - Sci. Eng. 50, 379–469.
Alfonso, D.R., 2008. First-principles studies of H_2S adsorption and dissociation on metal surfaces. Surf. Sci. 602, 2758–2768.
Spencer, M.S., 1999. The role of zinc oxide in Cu/ZnO catalysts for methanol synthesis and the water-gas shift reaction. Top. Catal. 8, 259–266.
Đnoğlu, N., Kitchin, J.R., 2009. Atomistic thermodynamics study of the adsorption and the effects of water-gas shift reactants on Cu catalysts under reaction conditions. J. Catal. 261, 188–194.
Zea, H., Lester, K., Datye, A.K., Rightor, E., Gulotty, R., Waterman, W., Smith, M., 2005. The influence of Pd–Ag catalyst restructuring on the activation energy for ethylene hydrogenation in ethylene-acetylene mixtures. Appl. Catal. A: Gen. 282, 237–245.
Bond, G.C., 1962. Catalysis by metals. Academic Press, New York, pp. 281–309.
Kim, S.K., Ji, H.L., Ahn, I.Y., 2011. Performance of Cu-promoted Pd catalysts prepared by adding Cu using a surface redox method in acetylene hydrogenation. Appl. Catal. A: Gen. 401, 12–19.
Khan, N.A., Shaikhutdinov, S., Freund, H.J., 2005. Acetylene and ethylene hydrogenation on alumina supported Pd-Ag model catalysts. Catal. Lett. 108, 159–164.
Sárkány, A., Horváth, A., Beck, A., 2002. Hydrogenation of acetylene over low loaded Pd and Pd-Au/SiO_2 catalysts. Appl. Catal. A: Gen. 229, 117–125.
Jin, Q., He, Y.F., Miao, M.Y., Guan, C.Y., Du, Y.Y., Feng, J.T., Li, D.Q., 2015. Highly selective and stable PdNi catalyst derived from layered double hydroxides for partial hydrogenation of acetylene. Appl. Catal. A: Gen. 500, 3–11.
Teschner, D., Borsodi, J., Wootsch, A., Revay, Z., Kaveckre, M., Knop-Gericke, A., Jackson, S.D., Schlögl, R., 2008. The roles of subsurface carbon and hydrogen in palladium-catalyzed alkyne hydrogenation. Science 320, 86–89.
Gabasch, H., Hayek, K., Knop-Gericke, A., Schlögl, R., 2006. Carbon incorporation in Pd(111) by adsorption and dehydrogenation of ethene. J. Phys. Chem. B 110, 4947–4952.
García-Mota, M., Bridier, B., Pérez-Ramírez, J., López, N., 2010. Interplay between carbon monoxide, hydrides, and carbides in selective alkyne hydrogenation on palladium. J. Catal. 273, 92–102.
Nikolaev, S.A., Zanaveskin, I.L.N., Smirnov, V.V., Averyanov, V.A., Zanaveskin, K.L., 2009. Catalytic hydrogenation of alkyne and alkadiene impurities from alkenes. Practical and theoretical aspects. Chem. Rev. 78, 231–247.
McKenna, F.M., Anderson, J.A., 2011. Selectivity enhancement in acetylene hydrogenation over diphenyl sulphide-modified Pd/TiO_2 catalysts. J. Catal. 281, 231–240.
McKenna, F.M., Wells, R.P.K., Anderson, J.A., 2011. Enhanced selectivity in acetylene hydrogenation by ligand modified Pd/TiO_2 catalysts. Chem. Commun. 47, 2351–2353.
McCue, A.J., Guerrero-Ruiz, A., Rodríguez-Ramos, I., Anderson, J.A., 2016. Palladium sulphide-A highly selective catalyst for the gas phase hydrogenation of alkynes to alkenes. J. Catal. 340, 10–16.
McCue, A.J., Guerrero-Ruiz, A., Ramirez-Barria, C., Rodríguez-Ramos, I., Anderson, J. A., 2017. Selective hydrogenation of mixed alkyne/alkene streams at elevated pressure over a palladium sulfide catalyst. J. Catal. 355, 40–52.
Liu, Y.N., McCue, A.J., Feng, J.T., Guan, S.L., Li, D.Q., Anderson, J.A., 2018. Evolution of palladium sulfide phases during thermal treatments and consequences for acetylene hydrogenation. J. Catal. 364, 204–215.
Shaikhutdinov, S., Heemeier, M., Bäumer, M., Lear, T., Lennon, D., Oldman, R.J., Jackson, S.D., Freund, H.J., 2001. Structure-reactivity relationships on supported metal model catalysts: Adsorption and reaction of ethene and hydrogen on Pd/Al2O3/NiAl(110). J. Catal. 200, 330–339.
Shao, L.D., Zhang, B.S., Zhang, W., Teschner, D., Girgsdies, F., Schlçgl, R., Su, D.S., 2012. Improved selectivity by stabilizing and exposing active phases on supported Pd nanoparticles in acetylene-selective hydrogenation. Chem. Eur. J. 18, 14962–14966.
Liu, Y.N., Fu, F.Z., McCue, A., Jones, W., Rao, D.M., Feng, J.T., He, Y.F., Li, D.Q., 2020. Adsorbate-induced structural evolution of Pd catalyst for selective hydrogenation of acetylene. ACS Catal. 10, 15048–15059.
Sá, J., Arteaga, G.D., Daley, R.D., Bernardi, J., Anderson, J.A., 2006. Factors influencing hydride formation in a Pd/TiO_2 catalyst. J. Phys. Chem. B 110, 17090–17095.

Doyle, A.M., Shaikhutdinov, S.K., Freund, H.J., 2004. Alkene chemistry on the palladium surface: Nanoparticles vs single crystals. J. Catal. 223, 444–453.
McCue, A.J., McRitchie, C.J., Shepherd, A.M., Anderson, J.A., 2014. Cu/Al_2O_3 catalysts modified with Pd for selective acetylene hydrogenation. J. Catal. 319, 127–135.
Bridier, B., Pérez-Ramírez, J., 2010. Cooperative effects in ternary Cu-Ni-Fe catalysts lead to enhanced alkene selectivity in alkyne hydrogenation. J. Am. Chem. Soc. 132, 4321–4327.
Garcia, M.A., Morse, M.D., 2013. Electronic spectroscopy and electronic structure of copper acetylide. CuCCH. J. Phys. Chem. A 117, 9860–9870.
Jana, G., Pan, S., Merino, G., Chattaraj, P.K., 2018. Noble gas inserted metal acetylides (Metal=Cu, Ag, Au). J. Phys. Chem. A 122 (37), 7391–7401.
Wilde, M., Fukutani, K., Ludwig, W., Brandt, B., Fischer, J.H., Schauermann, S., Freund, H.J., 2008. Influence of carbon deposition on the hydrogen distribution in Pd nanoparticles and their reactivity in olefin hydrogenation. Angew. Chem. Int. Ed. 47, 9289–9293.
Larsson, M., Jansson, J., Asplund, S., 1998. The role of coke in acetylene hydrogenation on Pd/α-Al_2O_3. J. Catal. 178, 49–57.
Sarkany, A., Weiss, A.H., Szilagyi, T., Sandor, P., Guczi, L., 1984. Green oil poisoning of a Pd/Al_2O_3 acetylene hydrogenation catalyst. Appl. Catal. 12, 373–379.
Sarkany, A., Guczi, L., Weiss, A.H., 1984. On the aging phenomenon in palladium catalysed acetylene hydrogenation. Appl. Catal. 10, 369–388.
Asplund, S., 1996. Coke formation and its effect on internal mass transfer and selectivity in Pd-catalysed acetylene hydrogenation. J. Catal. 158, 267–278.
Kyriakou, G., Boucher, M.B., Jewell, A.D., Lewis, E.A., Lawton, T.J., Baber, A.E., Tierney, H.L., Flytzani-Stephanopoulos, M., Sykes, E.C., 2012. Isolated metal atom geometries as a strategy for selective heterogeneous hydrogenations. Science 335, 1209–1212.
Larsson, M., Jansson, J., Asplund, S., 1996. Incorporation of deuterium in coke formed on an acetylene hydrogenation catalyst. J. Catal. 162, 365–367.
Yang, B., Burch, R., Hardacre, C., Hu, P., Hughes, P., 2014. Mechanistic study of 1,3-butadiene formation in acetylene hydrogenation over the Pd-based catalysts using density functional calculations. J. Phys. Chem. C 118, 1560–1567.
Borodzinski, A., Cybulski, A., 2000. A kinetic model of hydrogenation of acetylene–ethylene mixtures over a palladium surface covered by carbonaceous deposits. Appl. Catal. A: Gen. 198, 51–66.
Teschner, D., Vass, E., Havecker, M., Zafeiratos, S., Schnorch, P., Sauer, H., Knop-Gericke, A., Schlogl, R., Chamam, M., Wootsch, A., Canning, A.S., Gamman, J.J., Jackson, S.D., McGregor, J., Gladden, L.F., 2006. Alkyne hydrogenation over Pd catalysts: A new paradigm. J. Catal. 242, 26–37.
Huisgen, R., 1963. Kinetics and mechanism of 1,3-dipolar cycloadditions. Angew. Chem. Int. Ed. 2, 633–645.
Lee, J.W., Liu, X., Mou, C.Y., 2013. Selective hydrogenation of acetylene over SBA-15 supported Au-Cu bimetallic catalysts. J. Chin. Chem. Soc. 60, 907–914.
Maimaiti, Y., Nolan, M., Elliott, S.D., 2014. Reduction mechanisms of the CuO(111) surface through surface oxygen vacancy formation and hydrogen adsorption. PCCP 16, 3036–3046.
Zhang, R.G., Zhang, J., Zhao, B., He, L.L., Ling, L.X., Wang, B.J., 2017. Insight into the effects of Cu component and the promoter on the selectivity and activity for efficient removal of acetylene from ethylene on Cu-based catalyst. J. Phys. Chem. C 121, 27936–27949.
Zhang, R., Liu, H., Li, J., Ling, L., Wang, B., 2012. A mechanistic study of H_2S adsorption and dissociation on Cu_2O(111) surfaces: Thermochemistry, reaction barrier. Appl. Surf. Sci. 258 (24), 9932–9943.
Galtayries, A., Bonnelle, J.-P., 1995. XPS and ISS studies on the interaction of H_2S with polycrystalline Cu, Cu_2O and CuO surfaces. Surf. Interface Anal. 23 (3), 171–179.
Lin, J.Y., May, J.A., Didziulis, S.V., Solomon, E.I., 1992. Variable-energy photoelectron spectroscopic studies of H_2S chemisorption on Cu_2O and ZnO single-crystal surfaces: HS-bonding to copper(I) and zinc(II) sites related to catalytic poisoning. J. Am. Chem. Soc. 114, 4718–4727.
Delley, B., 1990. An all electron numerical method for solving the local density functional for polyatomic molecules. J. Chem. Phys. 92, 508–517.
Tian, D.X., Zhang, H.L., Zhao, J.J., 2007. Structure and structural evolution of Ag_n(n=3-22) clusters using a genetic algorithm and density functional theory method. Solid State Commun. 144, 174–179.
Halgren, T.A., Lipscomb, W.N., 1977. The synchronous-transit method for determining reaction pathways and locating molecular transition states. Chem. Phys. Lett. 49, 225–232.
Govind, N., Petersen, M., Fitzgerald, G., King-Smith, D., Andzelm, J., 2003. A generalized synchronous transit method for transition state location. Comput. Mater. Sci. 28, 250–258.
Yang, B., Burch, R., Hardacre, C., Headdock, G., Hu, P., 2013. Influence of surface structures, subsurface carbon and hydrogen, and surface alloying on the activity and selectivity of acetylene hydrogenation on Pd surfaces: A density functional theory study. J. Catal. 305, 264–276.
Wang, P., Yang, B.o., 2018. Influence of surface strain on activity and selectivity of Pd-based catalysts for the hydrogenation of acetylene: A DFT study. Chin. J. Catal. 39 (9), 1493–1499.
Wang, Y., Zheng, W.J., Wang, B.J., Ling, L.X., Zhang, R.G., 2021. The effects of doping metal type and ratio on the catalytic performance of C_2H_2 semi-hydrogenation over the intermetallic compound-containing Pd catalysts. Chem. Eng. Sci. 229, 116131.
Huang, F., Deng, Y.C., Chen, Y.L., Cai, X.B., Peng, M., Jia, Z.M., Xie, J.L., Xiao, D.Q., Wen, X.D., Wang, N., Jiang, Z., Liu, H.Y., Ma, D., 2019. Anchoring Cu_1 species over nanodiamond-graphene for semi-hydrogenation of acetylene. Nat. Commun. 10, 4431.
Zhang, R.G., Xue, M.F., Wang, B.J., Ling, L.X., 2019. Acetylene selective hydrogenation over different size of Pd-modified Cu cluster catalysts: Effects of Pd ensemble and cluster size on the selectivity and activity. Appl. Surf. Sci. 481, 421–432.
Zhang, R.G., Xue, M.F., Wang, B.J., Ling, L.X., Fan, M.H., 2019. C_2H_2 selective hydrogenation over the M@Pd and M@Cu (M=Au, Ag, Cu, and Pd) core-shell nanocluster catalysts: The effects of composition and nanocluster size on catalytic activity and selectivity. J. Phys. Chem. C 123, 16107–16117.
Islam, M.M., Diawara, B., Maurice, V., Marcus, P., 2009. Bulk and surface properties of Cu_2O: A first-principles investigation. J. Mol. Struct. (Thoechem) 903, 41–48.
Schulz, K.H., Cox, D.F., 1991. Photoemission and low-energy-electron-diffraction study of clean and oxygen-dosed Cu_2O(111) and (100) surfaces. Phys. Rev. B 43, 1610–1621.
Sun, B.Z., Chen, W.K., Zheng, J.D., Lu, C.H., 2008. Roles of oxygen vacancy in the adsorption properties of CO and NO on Cu_2O(111) surface: Results of a first-principles study. Appl. Surf. Sci. 255, 3141–3148.
Sun, B.Z., Chen, W.K., Wang, X., Lu, C.H., 2007. A density functional theory study on the adsorption and dissociation of N_2O on Cu_2O(111) surface. Appl. Surf. Sci. 253, 7501–7505.
Önsten, A., Göthelid, M., Karlsson, U.O., 2009. Atomic structure of Cu_2O(111). Surf. Sci. 603, 257–264.
Yin, S., Ma, X.Y., Ellis, D.E., 2007. Initial stages of H_2O adsorption and hydroxylation of Fe-terminated α-Fe_2O_3(0001) surface. Surf. Sci. 601, 2426–2437.
Zhang, R., Li, J., Wang, B., Ling, L., 2013. Fundamental studies about the interaction of water with perfect, oxygen-vacancy and pre-covered oxygen Cu_2O(111) surfaces: Thermochemistry, barrier, product. Appl. Surf. Sci. 279, 260–271.
Zhang, R.G., Liu, H.Y., Zheng, H.Y., Ling, L.X., Li, Z., Wang, B.J., 2011. Adsorption and dissociation of O_2 on the Cu_2O(111) surfaces: Thermochemistry, reaction barrier. Appl. Surf. Sci. 257, 4787–4794.
Zhang, R.G., Wang, B.J., Ling, L.X., Liu, H.Y., Huang, W., 2010. Adsorption and dissociation of H_2 on the Cu_2O(111) surfaces: A density functional theory study. Appl. Surf. Sci. 257, 1175–1180.
Yu, X.H., Zhang, X.M., Wang, S.G., Feng, G., 2015. A computational study on water adsorption on Cu_2O(111) surfaces: The effects of coverage and oxygen defect. Appl. Surf. Sci. 343, 33–40.
Wu, H.W., Zhang, N., Wang, H.M., Hong, S.G., 2012. First-principles study of oxygen-vacancy Cu_2O (111) surface. J. Theor. Comput. Chem. 11, 1261–1280.
Yang, B.o., Burch, R., Hardacre, C., Headdock, G., Hu, P., 2012. Origin of the increase of activity and selectivity of nickel doped by Au, Ag, and Cu for acetylene hydrogenation. ACS Catal. 2 (6), 1027–1032.
P. A. Sheth, M. Neurock, C. M. Smith, First-principles analysis of the effects of alloying Pd with Ag for the catalytic hydrogenation of acetylene-ethylene mixtures. J. Phys. Chem. B 109 (2005) 12449–12466.
Zhao, Z.J., Zhao, J.B., Chang, X., Zha, S.J., Zeng, L., Gong, J.L., 2019. Competition of C-C bond formation and C-H bond formation for acetylene hydrogenation on transition metals: A density functional theory study. AIChE J. 65, 1059–1066.
Cheng, J., Hu, P., 2011. Theory of the kinetics of chemical potentials in heterogeneous catalysis. Angew. Chem. Int. Ed. 50, 7650–7654.
Cheng, J., Hu, P., Ellis, P., French, S., Kelly, G., Lok, C.M., 2008. Brønsted-Evans-Polanyi relation of multistep reactions and volcano curve in heterogeneous catalysis. J. Phys. Chem. C 112, 1308–1311.
Zhang, R.G., Zhang, J., Jiang, Z., Wang, B.J., Fan, M.H., 2018. The cost-effective Cu-based catalysts for the efficient removal of acetylene from ethylene: The effects of Cu valence state, surface structure and surface alloying on the selectivity and activity. Chem. Eng. J. 351, 732–746.
Zhang, R., Zhao, B.o., He, L., Wang, A., Wang, B., 2018. Cost-effective promoter-doped Cu-based bimetallic catalysts for the selective hydrogenation of C_2H_2 to C_2H_4: The effect of the promoter on selectivity and activity. PCCP 20 (25), 17487–17496.